Hindawi
International Journal of Photoenergy
Volume 2019, Article ID 3810970, 15 pages
https://doi.org/10.1155/2019/3810970

Research Article

Comparison of the Performance of Photovoltaic Power Generation-Consumption System with Push-Pull Converter under the Effect of Five Different Types of Controllers

Hilmi Zenk

Department of Electrical-Electronics Engineering, Engineering Faculty, Giresun University, 28200 Giresun, Turkey

Correspondence should be addressed to Hilmi Zenk; hilmi.zenk@giresun.edu.tr

Received 20 July 2019; Revised 24 September 2019; Accepted 28 October 2019; Published 7 December 2019

Academic Editor: Francesco Riganti-Fulginei

In this study, a dynamic system has been modeled to efficiently use a photovoltaic generation and control system (PVGCS) for driving of a medium power off-grid electric machine. The measures have been taken to respond to three different disturbing factors in this system. First, the photovoltaic panels selected for energy generation have a variable solar radiation effect. Second, the DC motor load at the system output is assumed to have a variable torque. Third, a variable reference voltage, which is determined even in the case of time-varying energy generation and consumption of the system, is followed with minimum error. For this purpose, a push-pull converter has been chosen as a highly flexible structure since it is predicted that it can provide stable and effective variable DC voltage at increasing and decreasing level required for DC motor. The control of the DC voltage at different levels to be provided by the push-pull converter is performed by PI, fuzzy logic, fuzzy-tuned PI, 2-DOF PI, and fractional PID logic whose coefficients are selected by appropriate methods, respectively. The system efficiency and stability under the influence of these five different advanced controllers are compared. In the case of two disturbing factors affecting the system, the difference values (errors) of the voltage generated by each selected controller with the reference voltage are determined comparatively. The studies were carried out by using dynamic system modeling in MATLAB-SIMULINK software. In addition, the results of this study proved which type of controllers is more successful in controlling systems with the second order and more instability factors and which of them responds to sudden changes in errors more quickly.

1. Introduction

One of the most effective ways to produce electricity without harming the environment is through the use of solar energy. Solar energy is described in the photovoltaic event, which is converted to electrical energy. A photovoltaic event is a physical phenomenon defined as the transformation of sunlight into electrical energy. Solar cells are semiconductors which can convert sunlight directly into their electrical energy. The solar cell operating with this principle produces voltage on the ends depending on the amount of light falling on it. The voltage produced varies directly depending on the amount of incoming sunlight.

A number of solar cells are combined to form panels, and panels are combined to form PV power systems [1]. The output of solar panels is generated from DC electric energy. The DC voltage and power from solar panels can supply DC or AC loads with various power electronic converters.

Solar cells can be manufactured from many materials, such as amorphous silicon, copper indium gallium selenide, and cadmium telluride [2]. There are many studies on cost and efficiency in solar panels. The efficiency of the current photovoltaic panel has been expressed many times, reaching 35% [3]. In plants with large power generation from solar energy-producing countries, the development of solar panel manufacturing techniques has become more economical with an increase in production and an increase in panel power values and efficiency [4].

DC type electrical energy produced from photovoltaic solar panels must be converted into DC or AC electrical

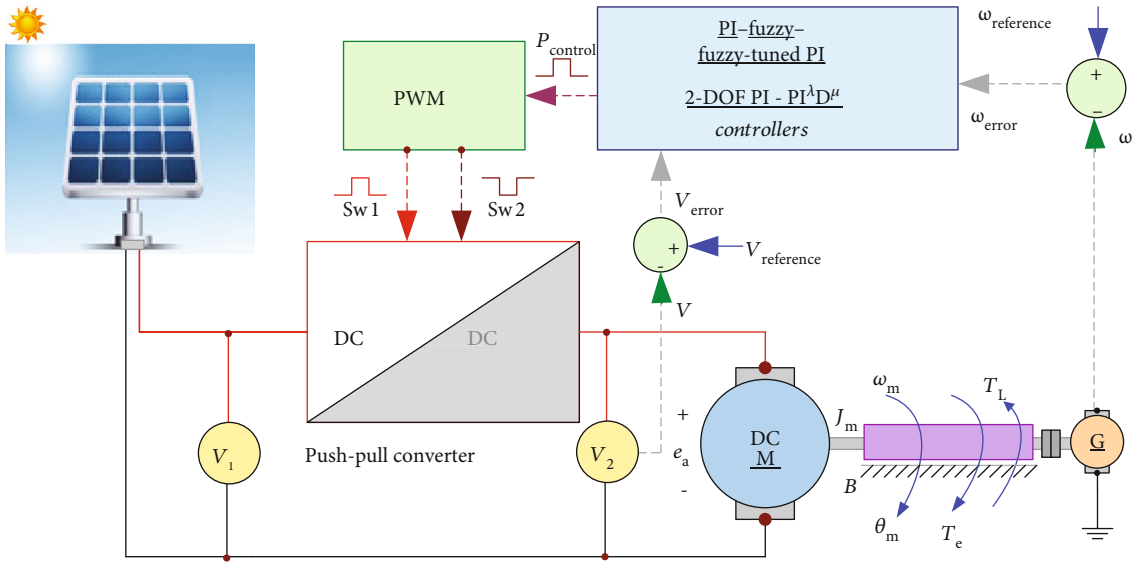

Figure 1: PVES with push-pull converter and DC motor.

energy according to the purpose of use. A different type of converter is required for this. However, the converters need a control system.

These converters are controlled by using classical and advanced control methods such as P, PI, PD, and PID controllers [5]; fuzzy logic controllers [6], fractional PID [7]; artificial neural networks [8]; vector control methods [9]; model predictive control [10]; and genetic algorithms [11].

In this study, an off-grid system is recommended. The photovoltaic solar power generation system in this network is connected to the push-pull converter. The performance of the push-pull converter is compared to the performances of PI, fuzzy, and fuzzy-tuned PI controllers, while feeding the DC motor-containing loads, respectively. In the simulation, it was tried to create difficult conditions by constantly changing the irradiation level of the sun coming into the panels. In this environment, the performances of the controllers were tested and the results were compared and the contribution of the advanced control techniques was discussed. The whole simulation was performed in a MATLAB/Simulink environment.

This paper is organized in four sections. Section 1 is the introduction. The designed push-pull converter, controllers, and DC motor load are described in Section 2. Section 3 presents the simulation results. The last section gives some remarks and conclusion.

2. Materials and Methods

The general scheme of the system consisting of push-pull transducer and DC motor connected to PI, fuzzy, fuzzy-tuned PI, 2-DOF PI, and fractional PID controllers, respectively, is proposed in Figure 1. The solar panels contained 40 parallel branches and 40 panels on each branch. The voltage from these panels feeds the DC motor with a push-pull type converter. The samples taken to control the voltage and speed of the motor in the desired reference

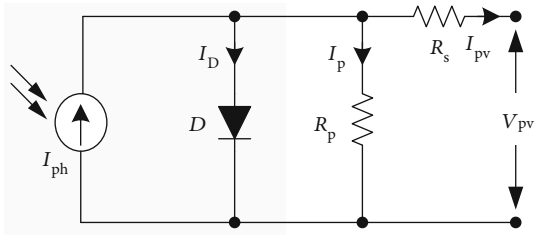

Figure 2: Equivalent circuit model of a PV solar cell.

range enter the controller unit. The control signals at the controller output turn into PWM signals and drive the push-pull converter switches.

2.1. PV Solar Cell Equivalent Circuit. Photovoltaic solar cells are semiconductor components that turn solar light to electrical energy [12]. In order to examine the behavior and electrical characteristics of photovoltaic solar cells, an equivalent circuit consisting of electrical circuit elements is needed [13]. Different equivalent circuit models for simple and advanced photovoltaic solar cells are found in the literature [14]. Because photovoltaic solar cells are not ideal elements, they are loss elements due to their physical structure. Therefore, losses are represented by resistances.

A commonly used equivalent circuit model for a photovoltaic solar cell is seen in Figure 2. The I_{ph} current source shows the current generated by the photons and is constant under constant radiation and temperature. The parallel R_p resistance is used to represent the leakage current and the series R_s resistance to the voltage drop in the output. The efficiency of the conversion in the photovoltaic battery is sensitive to small changes in R_s. However, it is not sensitive to changes in R_p. A small increase in R_s significantly reduces the output of the photovoltaic module [15]. The output

Table 1: The descriptions for PV cell.

Expression		Definition	Unit
V_{PV}	:	Cell output voltage	V
I_{PH}	:	Photocurrent, function of irradiation level, and junction of temperature	A
I_{PV}	:	Cell output current	A
I_{SC}	:	Cell short circuit current	A
I_0	:	Reverse saturation current	A
R_S	:	Series resistance of cell	Ω
N	:	Series cells per string	
λ	:	Constant coefficient depends upon the cell material	
M	:	Parallel strings	

voltage of the PV cell is shown in equation (1) [16]. Descriptions of the variables used here are seen in Table 1.

$$V_{PV} = \frac{N}{\lambda} \ln\left(\frac{I_{SC} - I_{PV} + MI_0}{MI_0}\right) - \frac{N}{M} R_s I_{PV}. \quad (1)$$

2.2. Push-Pull Converter. Figure 3 shows the circuit diagram of the dc-dc converter using the push-pull structure. In this circuit diagram, the symmetrical structure of the output stage is clearly visible. The circuit uses two active power switches. The converter uses a transformer for voltage trimming and electrical isolation, and the output inductor is used for energy storage. Therefore, unlike the design of the transformer for the single-ended converter, where care must be taken in selecting the core material and geometry to design for proper magnetizing inductance, in the push-pull converter, the transformer is used as an ideal element.

Since Sw_1 and Sw_2 share the current, the push-pull converter is used for higher power applications compared to the single-ended converters. Figure 4(a) illustrates the switching waveforms for Sw_1 and Sw_2 with a dead time during which both switches are open. The symmetrical structure of the push-pull stage permits two-sided use of the magnetic loop of the transformer [17]. The principle of push-pull converter operation is as follows. When the SW_1 switch is turned on, the current passes through the primary of the TR_1 transformer and the magnetic field at TR_1 expands along the core. This operating state is shown in Figure 4(b). The expanding magnetic field in TR_1 creates a voltage at the secondary TR_1; the polarity is inversely biased so that the D_2 diode is forward-oriented and the D_1 diode is cut. D_2 transmits and charges the output capacitor C through the L coil. L and C form an LC filter structure. The converter voltages are given by equation (2).

$$\begin{aligned} V_{s1} &= V_{s2} = V_i \frac{N_2}{N_1}, \\ V_{p1} &= V_{p2} = V_i, \\ V_L &= V_i \frac{N_2}{N_1} - V_o. \end{aligned} \quad (2)$$

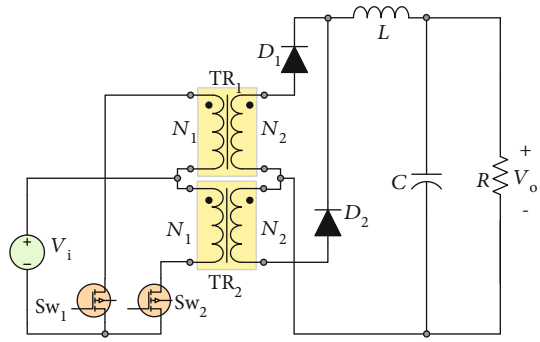

Figure 3: Equivalent circuit model of a push-pull converter.

When the Sw_1 switch is off, the magnetic field in TR_1 collapses, and after a dead time period (depending on the duty cycle of the PWM drive signal), the Sw_2 switch is transmitted; the current passes through the primer of TR_2, and the magnetic field at TR_2 expands along the core. This operating state is shown in Figure 4(c). At this point, the direction of the magnetic flux is reversed from that produced by the transmission state of Sw_1. The magnetic field emitted through the magnetic core forms a voltage in the secondary of TR_2; the polarity is in the opposite direction, leading to the D_1 diode and leading to the D_2 diode. When the D_1 diode is in transmission, C charges the output capacitor L. After some dead time, the Sw_1 switch is back to on and the cycle is repeated [18]. The converter new voltages are given by equation (3).

$$\begin{aligned} V_{s1} &= V_{s2} = -\frac{N_2}{N_1} V_i, \\ V_{p1} &= V_{p2} = -V_i, \\ V_L &= -V_{s2} - V_o = \frac{N_2}{N_1} V_i - V_o. \end{aligned} \quad (3)$$

There are two important considerations for the stable operation of push-pull converters. First, both switches should not be in the same position together, because this makes the source short circuit effectively. This means that the transmission time of each switch must not exceed half the total time for a full cycle; otherwise, the transmission will overlap. This operating state is shown in Figure 4(d). The duty cycle (D) must be less than 50% so that the switches do not have a coincidence. Second, the magnetic behavior of the transformers and switches in the circuit must be the same. Otherwise, the transformer may go to saturation and this will cause damage to the Sw_1 and Sw_2 switches. This behavior requires that the Sw_1 and Sw_2 keys have exactly the same individual transmission times and that the centers are magnetically balanced with the interconnected primary and secondary transformer ends. These criteria must be met by the transformer with the control and drive circuit. The output voltage (V_o) of the push-pull converter is equal to equation (4). Electrical parameters of the push-pull converter are given in Table 2.

$$V_o = 2DV_i \frac{N_2}{N_1}. \quad (4)$$

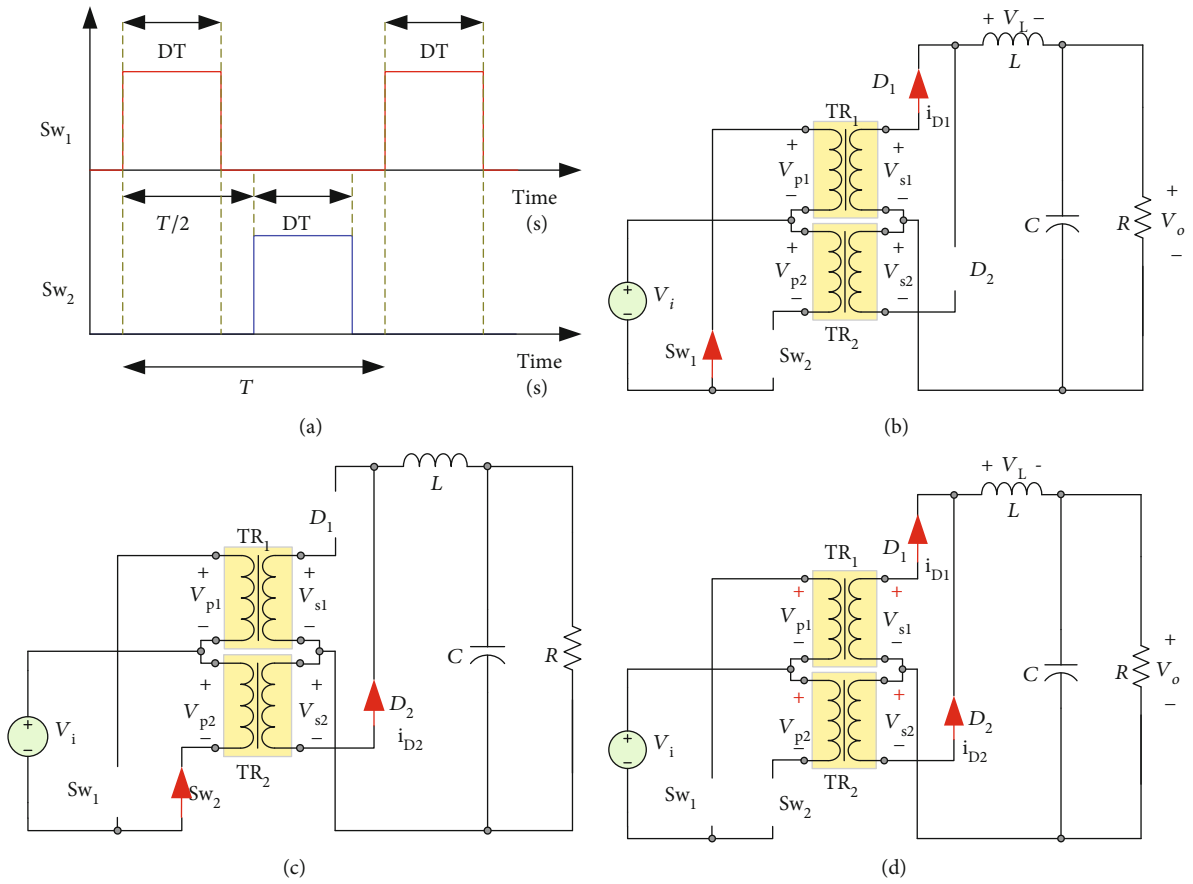

FIGURE 4: (a) Switching waveforms for Sw_1 and Sw_2. (b) Equivalent circuit when S_{W1} is on and Sw_2 is off. (c) Equivalent circuit when S_{W1} is off and Sw_2 is on. (d) Equivalent circuit when S_{W1} is off and Sw_2 is off.

TABLE 2: Push-pull converter parameters.

Expression		Definition	Value
V_i	:	Converter input voltage	0-1 kV
V_o	:	Converter output voltage	0-600 V
N_1	:	Number of secondary windings	1000 turns
N_2	:	Number of secondary windings	600 turns
L	:	Inductor	1 mH
C	:	Capacitor	10 mF
f_{Sw}	:	Switch frequency	1 kHz

2.3. DC Motor Model. Many features that are required to be in a motor are available in a DC motor. Some of these features include safety, durability, and cheapness and low voltage levels. DC motors are preferred in many applications. The electrical circuit and the electrical circuit diagram of the rotor of a direct current motor are shown in Figure 5. The parameters and symbols used in the system are given in Table 3.

According to Kirchhoff's voltage law, the electrical equation of the DC motor is given in equation (5). Here, $i_a(t)$ is the armature current, $e_a(t)$ is back voltage, and $V_s(t)$ is the voltage source. In equation (6), the back emf voltage $e_a(t)$ is expressed to be proportional to a constant, such as K_e, with the angular velocity of the rotor $\omega(t)$ in the motor. Furthermore, the torque generated by the motor, T_m, is calculated by multiplying the torque constant K_t by the armature current as shown in equation (7).

$$V_s(t) = R_a \cdot i_a(t) + L_a \frac{di_a(t)}{dt} + e_a(t), \tag{5}$$

$$e_a(k) = K_e \cdot \omega_m(t), \tag{6}$$

$$T_m(t) = K_t \cdot i_a(t). \tag{7}$$

θ is the position of the shaft, and T_L is the external load torque. The total torque of the motor must be zero; this is expressed in equation (8).

$$\frac{d\theta}{dt} = \dot{\theta} = \omega_t,$$
$$J_m \frac{d\omega_m}{dt} + B\omega_m = K_t \cdot i_a - B\omega_m - T_L. \tag{8}$$

2.4. PI Controller. The PI controller structure is simple and has a controller structure that provides very good results for many control systems. The control block diagram of the classical PI controller is given in Figure 6. In this configuration, the control signal $u(t)$ is the sum of two terms. Each of these

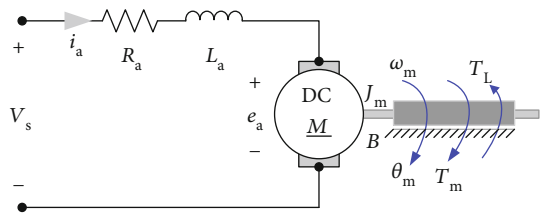

Figure 5: Basic structure of DC motor equivalent circuit.

Table 3: DC motor parameters.

Expression		Definition	Unit	
R_a	:	Armature resistance	Ω	2.581
L_a	:	Armature inductance	H	0.028
R_f	:	Field resistance	Ω	281.3
L_f	:	Field inductance	H	156
L_{af}	:	Field-armature mutual inductance	H	0.9483
J_m	:	Total inertia	kg·m^2	0.02215
B	:	Viscous friction coefficient	N·m·s	0.002953
T	:	Coulomb friction torque	N·m	0.5161
ωr_{start}	:	Initial speed	rad/s	1
If_{start}	:	Initial field current	A	1

terms is a function of the tracking error $e(t)$. The term K_p indicates that this term is proportional to the error. The term K_i/s is an integral term. Each of the terms works independently of the other. According to DC converter reference voltage input circuit, output voltage is controlled by the PI controller. Activated equations are as follows:

$$u(t) = K_p e(t) + K_i \int e(t)dt, \tag{9}$$

$$\frac{du(t)}{dt} = K_p \frac{de(t)}{dt} + K_i e(t). \tag{10}$$

If equation (10) is converted from the continuous time space t into the discrete time space k, then equation (11) is obtained.

$$\frac{u(k) - u(k-1)}{T_s} = K_p \frac{e(k) - e(k-1)}{T_s} + K_i e(k),$$
$$u(k) = u(k-1) + K_p[e(k) - e(k-1)] + K_i e(k). \tag{11}$$

The optimal P and I coefficients for the PI controller in this system were found by using the closed loop Ziegler-Nichols method.

2.5. Fuzzy Logic Controller (FLC). Fuzzy logic control algorithm is based on digitizing a set of heuristic control rules. It is important to note that fuzzy logic is used to evaluate uncertain, fuzzy sets and rules for expressing linguistic terms [19, 20]. The most important feature that distinguishes the concept of the fuzzy set from that of the classical set is that verbal variables are used instead of numerical variables. A fuzzy logic controller system is generally shown in Figure 7. As is known, the structure of the fuzzy logic controller consists of three parts. These sections are briefly mentioned in the "fuzzification" system phase, and the data obtained from the system are converted to fuzzy values. The second stage is "rule base," where fuzzy data is processed by fuzzy rules. In the last stage, which is called "defuzzification," the data is converted to the exact number of fuzzy results.

The knowledge base unit consists of two units, the database and the rule base. The knowledge base can be divided into two parts: the database, in which the decision-making unit receives the information used in the rule base, and the rule base, where there are linguistic control rules for audit purposes. The set of rules determines the audit objectives and audit strategy. Information about the system being audited, fuzzification, processing of fuzzy data, membership function required during defuzzification operations, and rule table information are available in the "database" unit. Connections between inputs and outputs are established using rules in the rule base. In a system, e and de are inputs, and if μ is the output variable (if $e = x$ and $de = y$, then $u = z$), defined by the rule, e and f take the value of the fuzzy value of the output determined. The rule table is shown in Figure 8.

2.6. Fuzzy-Tuned PI Controller (FT-PIC). The simplified block diagram of the fuzzy-tuned PI controller is shown in Figure 9. Membership functions for this controller type input error (e), change of error (de), and controller output (du) are defined on the normalized domain [-1, 1] as shown in Figure 10. Membership functions (MF) of β are defined on [0, 1] as shown in Figure 11.

Symmetric triangles with equal base width and 50% overlap with neighboring MFs are used here due to its natural and unbiased nature. The term sets of e, de, and du for PI type FLC contain the same linguistic expressions for the magnitude part of the linguistic values [21].

The operation of a PI-type FLC as shown in Figure 9 can be described by equation (12). Here, du is the incremental change in controller output. FT-PIC generates the nonlinear controller output (du) by modifying the output of the simple fuzzy-tuned PI controller (FT-PIC) as shown in Figure 9 and equation (13).

$$u(k) = u(k-1) + du(k), \tag{12}$$

$$du = \beta Gu(du_N 1). \tag{13}$$

The weighted absolute average of the effective rules of the controller can be taken as the absolute output. For this rinsing process, the central method of areas where the center of gravity of the active areas given in equation (14) is taken can be used.

$$du(k) = u \frac{\sum_{i=a,b,c,d} \mu_{Ri}(du_R) du_R(Ri)}{\sum_{i=1}^{n} uV_R}. \tag{14}$$

where k is the sampling time, m is the degree of membership, $e(k)$ is the control error, and (k) is the variation of this error in a sampling time. The Simulink model of the membership function related to weight coefficients according to the

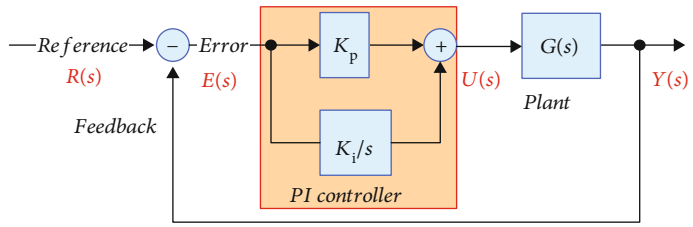

Figure 6: PI controller block diagram.

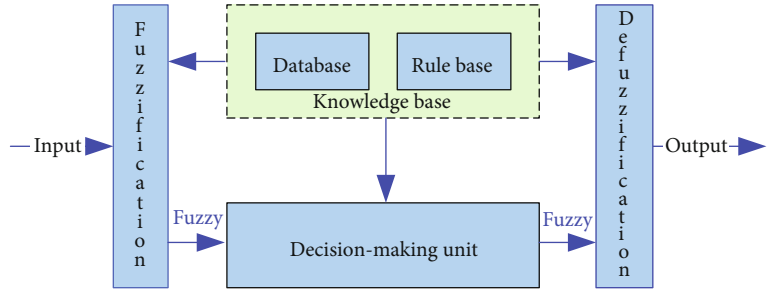

Figure 7: Basic configuration of a FLC.

de / e	N	Z	P
N	P	P	Z
Z	P	Z	N
P	Z	N	N

Figure 8: Rule base table.

expression in the share portion of the central method of the fields given by equation (14) was prepared as shown in Figure 12.

2.7. Two Degree Of Freedom (2-DOF) PI Controller. As with most industrial control applications, the desired value of the controlled variable or setpoint normally remains constant and needs to be changed. This control technique is mainly concerned with two free-grade (2-DOF) applications of PID control algorithms. The 2-DOF control algorithm provides additional parameter and regulative control performance, and the closed loop control system durability in mind to improve servo control behavior is used [22–26]. It is possible to incorporate this capability of Two Degree Of Freedom controllers into both PI-type and PID-type control algorithms.

The 2-DOF controller structure has been developed for situations where a 1-DOF controller structure is insufficient. By adding the β parameter to the controller structure, better performance is achieved in terms of maintaining reference distortion suppression performance and improving transient response. The structure of the 2-DOF PI controller is shown in Figure 13.

The control signal for the 2-DOF PI controller is given in equation (15). Here, T_i shows the integral time constant, T_d the derivative time constant, K_P proportional gain, β reference weight ratio, $C_r(s)$ reference signal transfer function, and $C_y(s)$ feedback transfer function [27].

$$u(k) = K_P\left(\beta + \frac{1}{T_i k}\right) r(k) - K_P\left(1 + \frac{1}{T_i k}\right) y(k),$$
$$u(k) = C_r(k) r(k) - C_y(k) y(k). \tag{15}$$

2.8. Fractional PID Controller ($PI^{\lambda}D^{\mu}$). Fractional type PID controllers can be described as the generalized form of PIDs. The output data can be summarized as a linear combination of the input, a fractional derivative of the input, and a fractional integral of the input [28]. Fractional PIDs are also known as $PI^{\lambda}D^{\mu}$ controllers, where λ and μ are the integration and differentiation orders; if both values are 1, the result is a usual PID (henceforth called "integer" PID as opposed to a fractional PID). $PI^{\lambda}D^{\mu}$ controllers are advanced controllers that can give better results than classical PI controllers. They are widely used because they are able to adjust more precisely than PID controllers. The best knowns are the descriptions of Shah and Agashe and Rasoanarivo and Sargos [29, 30]. The $PI^{\lambda}D^{\mu}$ controller general block diagram is shown in Figure 14.

In this study, λ and $\mu \geq 0$, where λ is the order of integration and μ is the order of differentiator. K_P, K_I, and K_D are the PID controller gains. $U(s)$ and $E(s)$ are the control and error signals, respectively. In this study, $PI^{\lambda}D^{\mu}$ controller software was performed by FOMCON Toolbox [31]. System output, $C(k)$, is as seen in

$$C(k) = K_P + \frac{K_I}{k^{\lambda}} + K_D k^{\mu}. \tag{16}$$

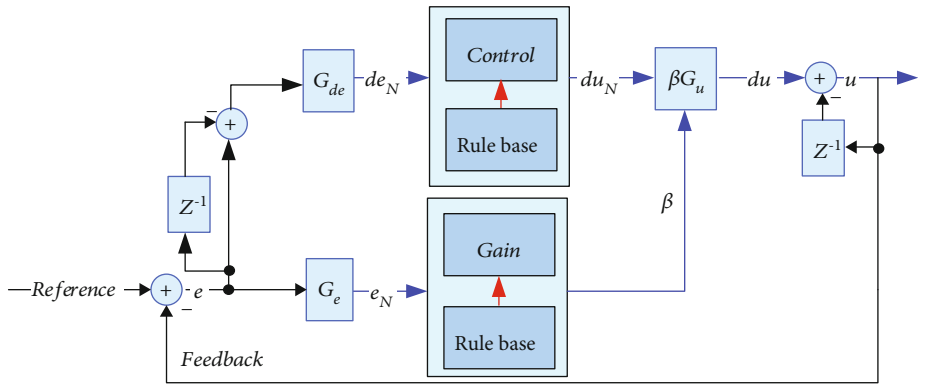

Figure 9: Basic configuration of a FT-PIC.

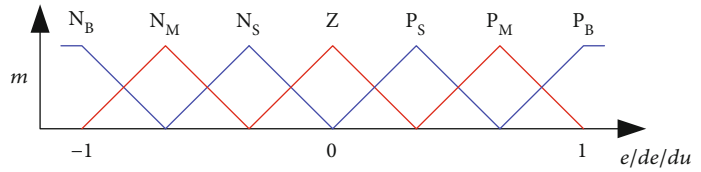

Figure 10: Membership functions of inputs (e, de) and output (du). $L_e = L_{de} = L_{du}$ (N_B: negative big; N_M: negative medium; N_S: negative small; Z: zero; P_S: positive small; P_M: positive medium; P_B: positive big).

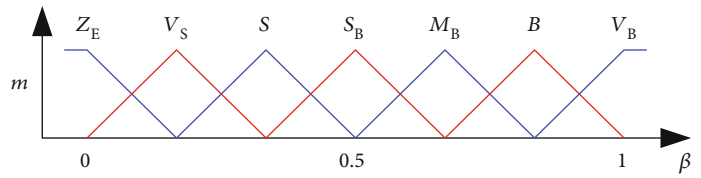

Figure 11: Membership functions of gain updating factor, β, are mapped {Z_E, V_S, S, S_B, M_B, B, V_B}.

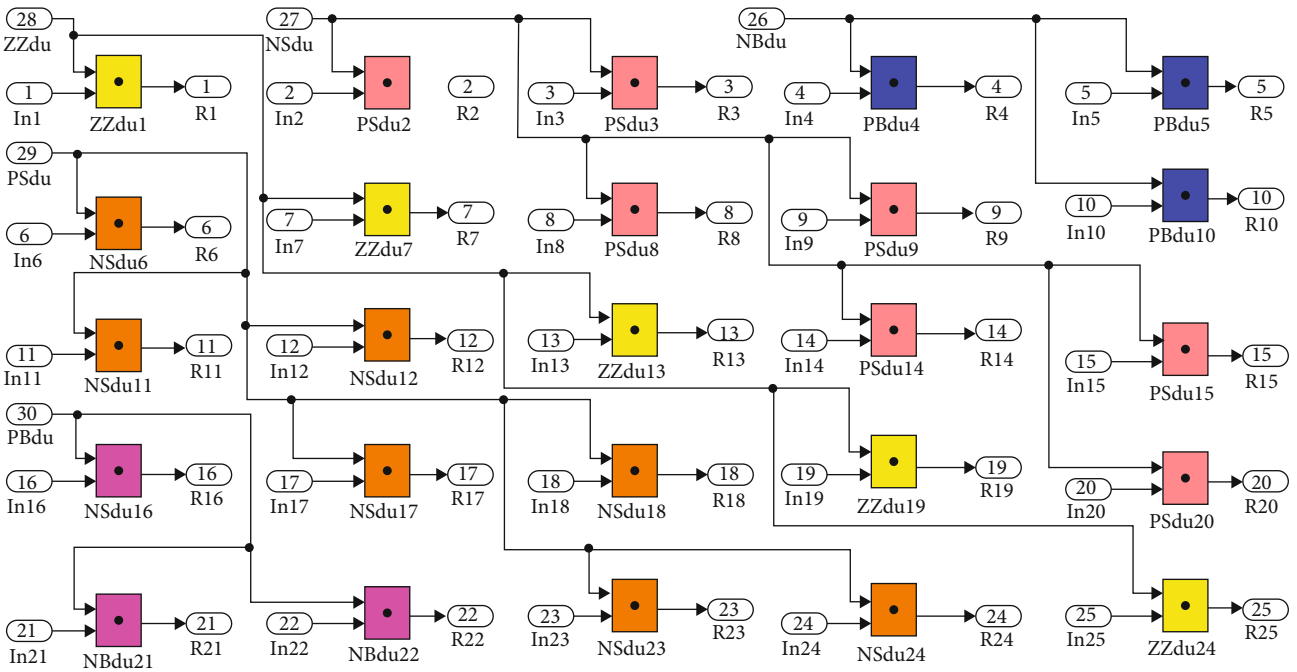

Figure 12: Simulink model of the central method of fields.

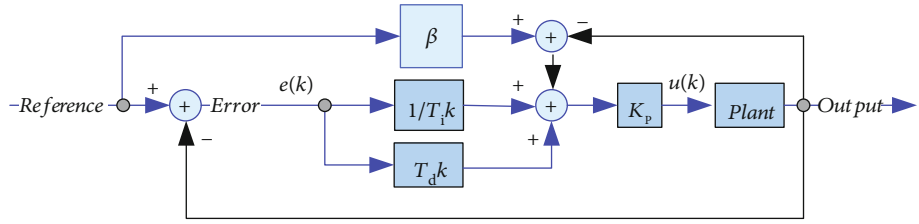

Figure 13: 2-DOF PI structure.

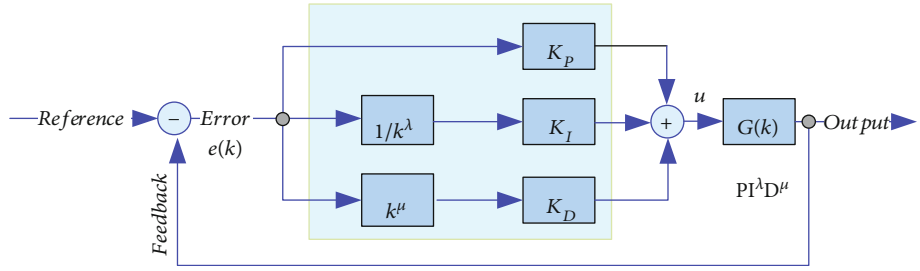

Figure 14: General block diagram of $PI^{\lambda}D^{\mu}$ structure.

3. Results and Discussion

First, the installed system was run uncontrolled. What happened in this case was investigated. Afterwards, PI, FLC fuzzy-tuned PI, 2-DOF PI, and fractional PID controllers are connected to the push-pull convertor connected system, and their results are shown. In all simulations, the solar radiation from the photovoltaic solar panels and the power of the drawn load were compared under the same conditions. In many practical applications, the system with the push-pull converter and fuzzy logic or PI controller gives the same results as computer simulations [32, 33].

3.1. Data of PV Panels. The selected solar panel is a BP SX3190 model and is easily available from the market. Table 4 shows the information regarding silicon nitride multi crystalline silicon cell high efficiency photovoltaic module. In all simulations, the solar radiation level at 25°C ambient temperature is shown in Figure 15.

For a PV powered power system that does not have a battery pack, it is not possible to achieve voltage stability of the loads with large solar radiation changes in 5 seconds. However, in this study, it also helps to show a good way to measure the response of the system to sudden power changes. The voltage stability of the push-pull converter used in the system is also examined under the variable load moment which is another disturbance under these radiation conditions. Comparing the five selected controllers in terms of system stability is very important for many practical applications.

3.2. Simulation Results and Discussion. The push-pull converter in the system is connected to the PI, FLC fuzzy-tuned PI, 2-DOF PI, and fractional PID controllers by manual switches. The reference voltage applied to these controllers is given in Figure 16. It provides the voltage error between the reference voltage and the output voltage signal produced by the push-pull converter, which enables the transmission of power to the secondary winding by generating electrical docks for the primary windings of the transformers according to the PWM method with the control voltage of the control signals. According to the type of feedback signal of the controllers, the DC motor can control the voltage, current, torque, or speed effectively.

Table 4: Photovoltaic solar panel parameters [34].

Value	Unit
Open circuit voltage	30.6021 V
Short-circuit current	8.51029 A
Maximum power	190 W
Voltage at maximum power point	24.3003 V
Current at maximum power point	7.82945 A
Temperature coefficient of short circuit current	0.065 ± 0.015%/°C
Temperature coefficient of open circuit voltage	-111 ± 10 mV/°C
Serial resistance	0.17514 ohm
Parallel resistance	755.51 ohm
Diode saturation current	1.0647*e*-6 A
Diode ideality factor	1.5

The sampling time of the system is 50 μs. The output voltage of the PV panels ranges from 1000 V to 1225 V, and the output current is up to 240 A. The changes in the torque taken by the load connected to the motor in the system are shown in Figure 17.

The controllers controlling the push-pull converter are connected to the pulse generator, which operates a pair of pulse width modulation principles. The frequency of these pulse generators working with reverse pulse logic is 1 kHz

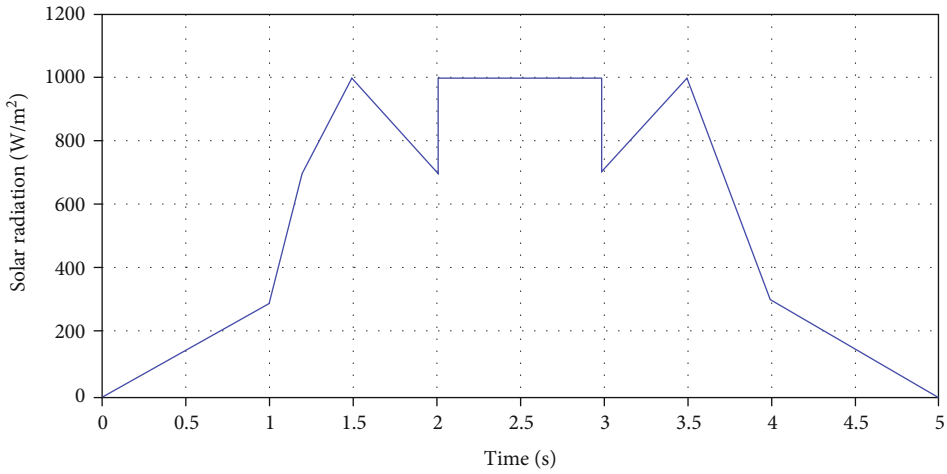

Figure 15: Ambient solar irradiation level changes.

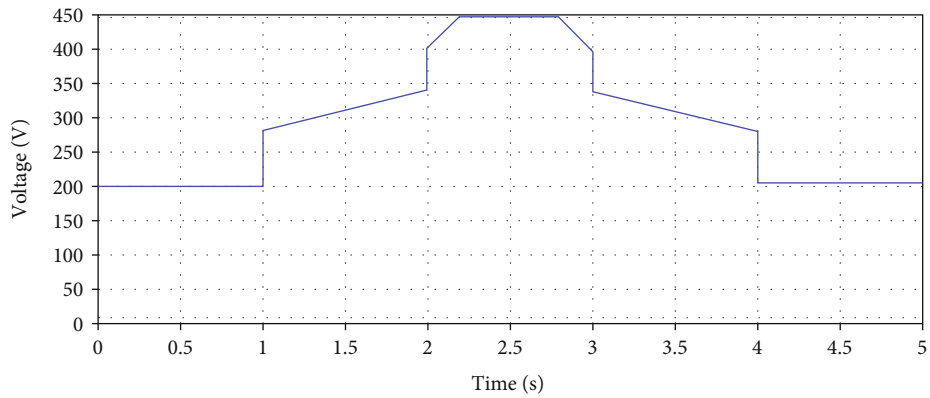

Figure 16: The reference voltage.

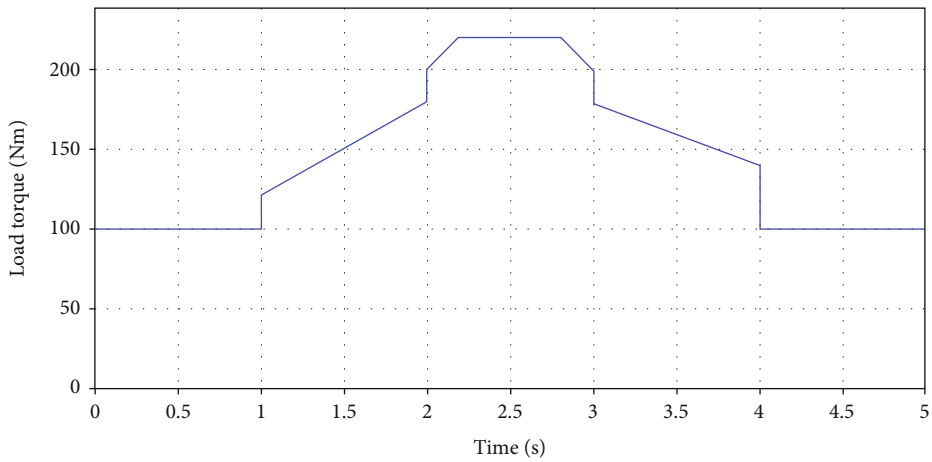

Figure 17: Time change of load torque (T_L) applied to DC motor.

and depends on the transformers by means of power electronics switches.

3.2.1. Case 1: Push-Pull Converter with PI Controller. The results obtained when the indirect current control method with the PI controller is used to control of the push-pull converter output voltage signals are shown Figure 18. The PI controllers used in the indirect current control method of the system under variable ambient conditions and constant change in load were set to $K_P = 10$ and $K_I = 100$. This

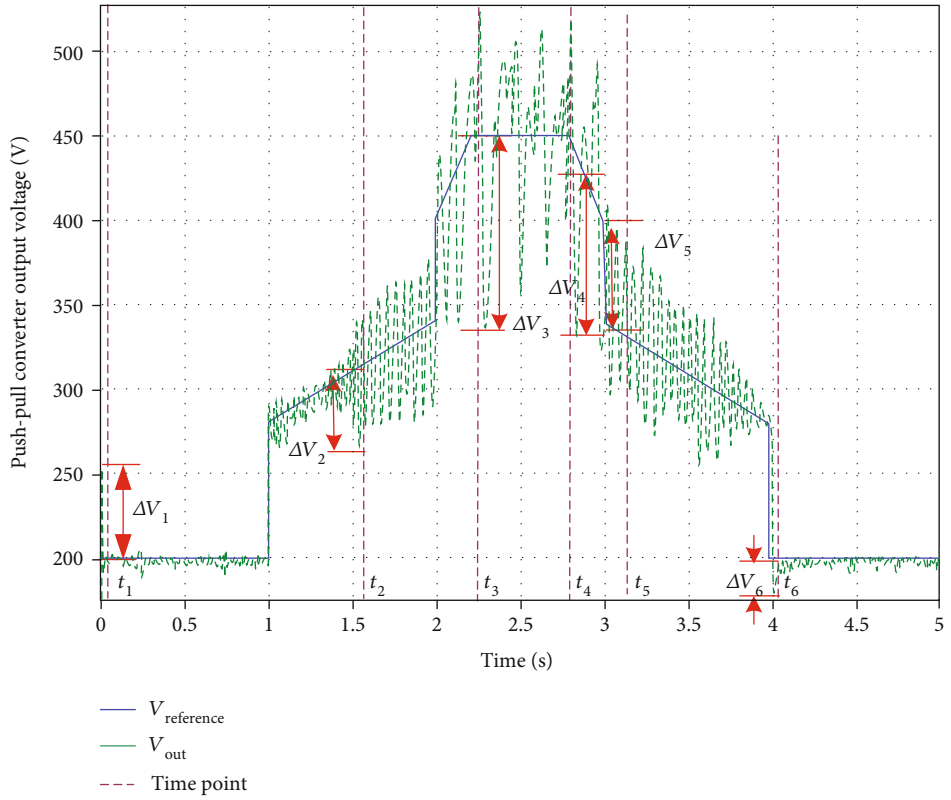

Figure 18: Push-pull converter output voltage signal connected to PI controller and overvoltage values at some points.

Table 5: Percentage (%) of error between output voltage and reference of the system.

Point number	Time (s)	Output voltage (V_o)	Reference voltage (V_{ref})	$\Delta V = V_{ref}$-V_o	% error
1	0.0600	255.40	200.00	-55.40	-27.70
2	1.5400	264.76	321.50	56.74	17.65
3	2.2800	336.32	450.00	113.68	25.26
4	2.8300	332.11	441.59	109.48	24.79
5	3.0720	428.34	335.68	-92.66	-27.60
6	4.0200	180.30	200.00	19.7	9.85

coefficients for the system were found by using the closed loop Ziegler-Nichols method.

Table 5 shows the output voltage signal of the push-pull converter connected to the PI controller shown in Figure 18 and the overvoltage values at some points.

The error voltage (ΔV) between the reference and output voltage signals in the Push-pull converter system with PI controller has been monitored. Accordingly, the five points where the error voltage is greatest is selected and it is calculated to be 22.14% when the percentage averages are taken according to the reference voltage.

3.2.2. Case 2: Push-Pull Converter with Fuzzy Logic Controller. The results obtained when the indirect current control method with the fuzzy logic controller is used to control of the push-pull converter output voltage signals are shown Figure 19.

Table 6 shows the output voltage signal of the push-pull converter connected to the FL controller shown in Figure 19 and the overvoltage values at some points. The error voltage (delta) between the reference and output voltage signals in the Push-pull converter system with FL controller has been monitored. Accordingly, the six points where the error voltage is greatest is selected and it is calculated to be 12.52% when the percentage averages are taken according to the reference voltage.

3.2.3. Case 3: Push-Pull Converter with Fuzzy-Tuned PI Controller. The results obtained when the indirect current control method with the fuzzy-tuned PI controller is used to control of the push-pull converter output voltage signals are shown Figure 20.

Table 7 shows the output voltage signal of the push-pull converter connected to the fuzzy-tuned PI controller shown

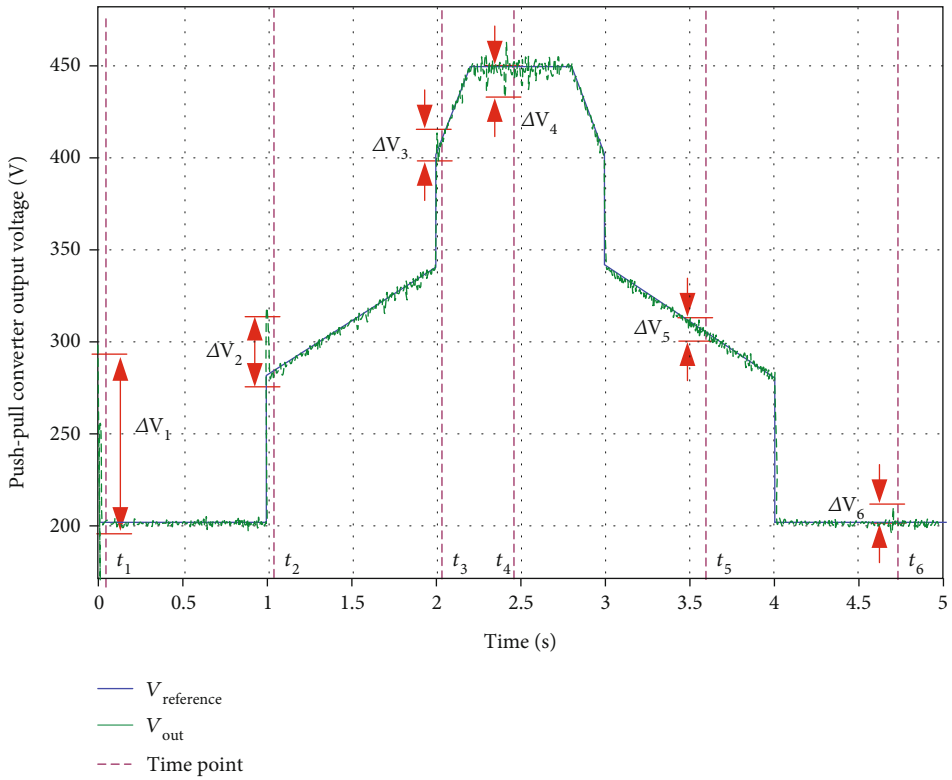

Figure 19: Push-pull converter output voltage signal connected to fuzzy logic controller and overvoltage values at some points.

Table 6: Percentage (%) of error between output voltage and reference of the system.

Point number	Time (s)	Output voltage (V_o)	Reference voltage (V_{ref})	$\Delta V = V_{ref}$-V_o	% error
1	0.0065	297.72	200.00	-97.72	-48.86
2	1.006	317.84	280.36	-37.48	-13.37
3	2.0054	414.46	401.36	-13.1	-3.26
4	2.4133	433.63	450.00	16.37	3.64
5	3.5679	283.00	287.93	4.93	1.71
6	4.0200	200.00	209.02	9.02	4.32

in Figure 20 and the overvoltage values at some points. The error voltage (delta) between the reference and output voltage signals in the Push-pull converter system with fuzzy-tuned PI controller has been monitored. Accordingly, the six points where the error voltage is greatest is selected and it is calculated to be 15.99% when the percentage averages are taken according to the reference voltage.

3.2.4. Case 4: Push-Pull Converter with 2-DOF PID Controller. The results obtained when the indirect current control method with the 2-DOF PI controller is used to control of the push-pull converter output voltage signals are shown Figure 21.

Table 8 shows the output voltage signal of the push-pull converter connected to the 2-DOF PI controller shown in Figure 21 and the overvoltage values at some points. The error voltage (delta) between the reference and output voltage signals in the Push-pull converter system with 2-DOF PI controller has been monitored. Accordingly, the six points where the error voltage is greatest is selected and it is calculated to be 18.94% when the percentage averages are taken according to the reference voltage.

3.2.5. Case 5: Push-Pull Converter with Fractional PID ($PI^{\lambda}D^{\mu}$) Controller. The results obtained when the indirect current control method with the $PI^{\lambda}D^{\mu}$ controller is used to control of the push-pull converter output voltage signals are shown Figure 22. Table 9 shows the output voltage signal of the push-pull converter connected to the $PI^{\lambda}D^{\mu}$ controller shown in Figure 22 and the overvoltage values at some points.

The error voltage (delta) between the reference and output voltage signals in the Push-pull converter system with P $I^{\lambda}D^{\mu}$ controller has been monitored. Accordingly, the five

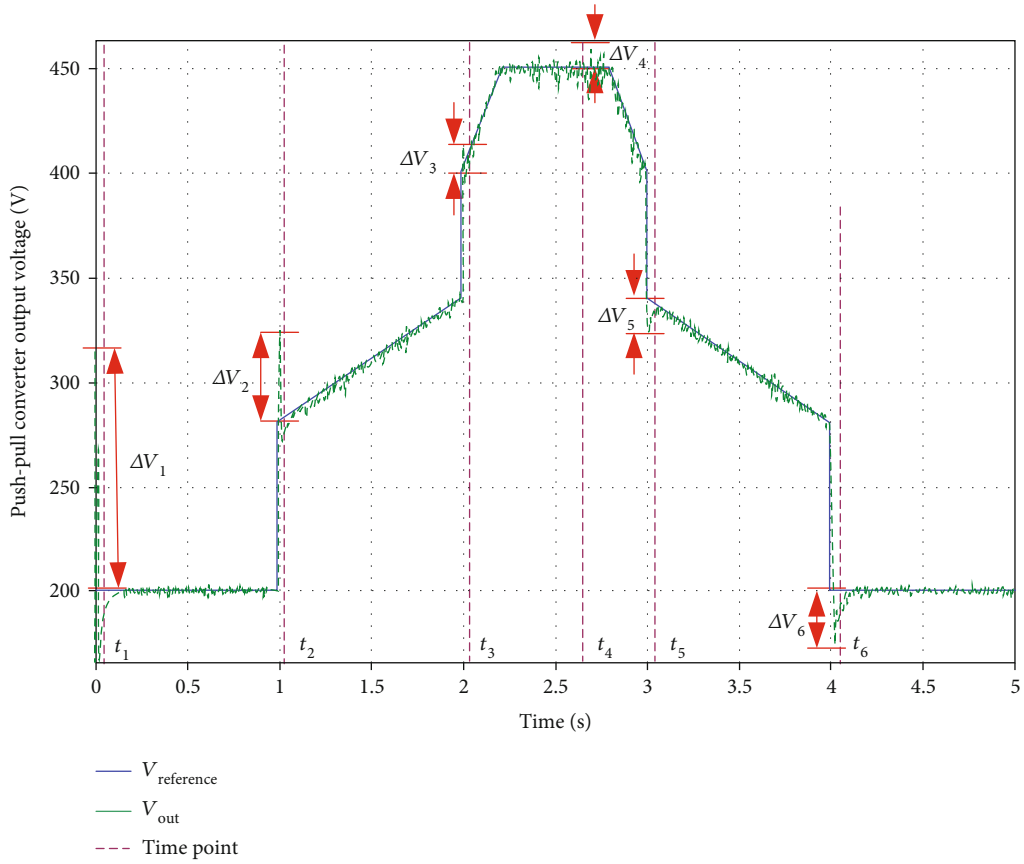

Figure 20: Push-pull converter output voltage signal connected to fuzzy-tuned PI controller and overvoltage values at some points.

Table 7: Percentage (%) of error between output voltage and reference of the system.

Point number	Time (s)	Output voltage (V_o)	Reference voltage (V_{ref})	$\Delta V = V_{ref}$-V_o	% error
1	0.0064	314.13	200.00	-114.13	-57.07
2	1.0530	324.90	280.30	-44.60	-15.91
3	2.0034	412.90	400.85	-12.05	-3.01
4	2.6900	461.39	450.00	-11.39	-2.53
5	3.0135	323.67	339.19	15.52	4.58
6	4.0200	174.33	200.00	25.67	12.84

points where the error voltage is greatest is selected and it is calculated to be 18.78% when the percentage averages are taken according to the reference voltage.

Table 10 gives the average of the percent (% e) of the absolute value of the error between the output voltage produced by the five different controllers obtained from the simulations and the reference of the system.

4. Conclusion

In the study, the performance of the system connected to the push-pull converter was investigated using different controllers. The success of the system is to compare the variable load current demand with variable reference voltage in the variable solar radiation of the loads fed by the grid independent solar panels.

The energy generation of the system is provided by photovoltaic solar panels. However, during the simulation, there is production under a variable solar radiation. The load of the system is designed as a DC motor which draws a lot of current. If the system design is made a little more difficult and the third variable is the push-pull converter, the output voltage is required to follow the reference given. Under these variables, PI, fuzzy logic, fuzzy-tuned PI-based, 2-DOF PI, and fractional PID control elements were the successors of the control system.

Fuzzy logic and fuzzy-tuned PI-based controllers were the most effective of the reference signal from these controllers. It was seen that these two controllers were removed from the total of six points during the 5-second simulation. There is no significant difference between the percentages of voltage differences at these points. However, the classic fuzzy-based

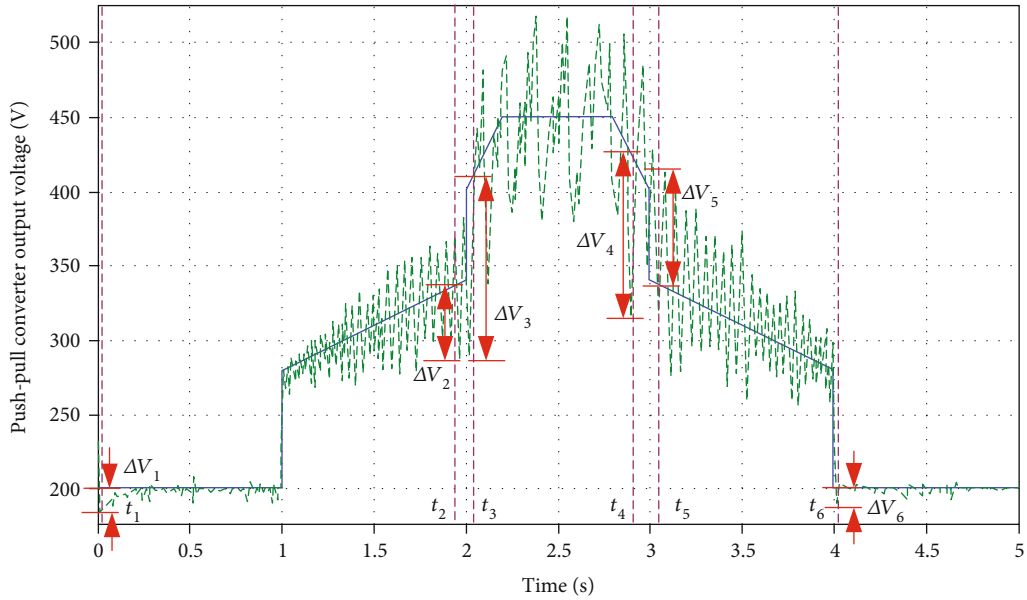

Figure 21: Push-pull converter output voltage signal connected to 2-DOF PI controller and overvoltage values at some points.

Table 8: Percentage (%) of error between output voltage and reference of the system.

Point number	Time (s)	Output voltage (V_o)	Reference voltage (V_{ref})	$\Delta V = V_{ref} - V_o$	% error
1	0.0061	234.28	200.00	-34.28	-17.14
2	1.7332	276.93	324.00	47.07	14.53
3	2.0190	289.42	404.72	115.30	28.49
4	2.8945	313.95	426.42	112.47	26.38
5	3.1420	403.50	331.48	-72.02	-21.73
6	4.0175	189.31	200.00	10.69	5.35

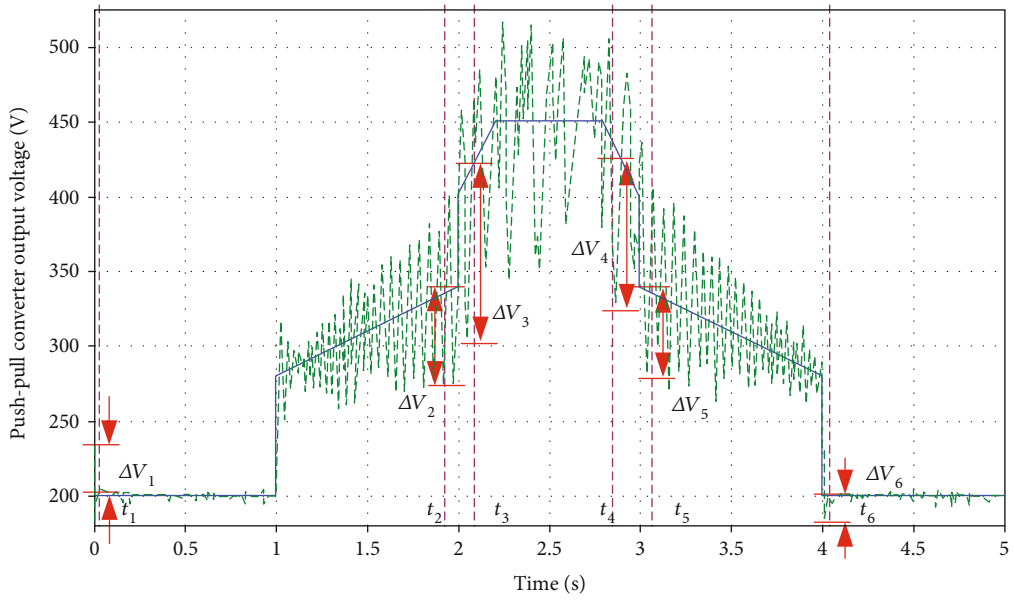

Figure 22: Push-pull converter output voltage signal connected to $PI^{\lambda}D^{\mu}$ controller and overvoltage values at some points.

Table 9: Percentage (%) of error between output voltage and reference of the system.

Point number	Time (s)	Output voltage (V_o)	Reference voltage (V_{ref})	$\Delta V = V_{ref} - V_o$	% error
1	0.0070	233.19	200.00	-33.19	-16.60
2	1.9765	274.69	338.58	63.89	18.87
3	2.0525	303.18	413.12	109.94	26.61
4	2.8660	327.61	433.36	105.75	24.40
5	3.1605	270.00	330.35	60.35	18.27
6	4.0247	184.10	200.00	15.90	7.95

Table 10: Average of the percentages (%e) of the absolute value of the error between the output voltage produced by the five different controllers and the reference of the system.

Point number	PI	Fuzzy logic (FLC)	Fuzzy-tuned PI (FT-PIC)	2-DOF PI	Fractional PID ($PI^{\lambda}D^{\mu}$)
1	-27.70	-48.86	-57.07	-17.14	-16.60
2	17.65	-13.37	-15.91	14.53	18.87
3	25.26	-3.26	-3.01	28.49	26.61
4	24.79	3.64	-2.53	26.38	24.40
5	-27.60	1.71	4.58	-21.73	18.27
6	9.85	4.32	12.84	5.35	7.95
(% e)	**22.14**	**12.53**	**15.99**	**18.93**	**18.78**

controller (FLC) performed slightly better. The most failed controller was the PI controller.

During the simulations, large fault voltages were observed many times in all of the controllers. The point with a high error voltage occurred at the beginning of the simulation. However, based on the selected points, the FT-PIC gave a large error voltage of 57.07%. Considering all this information, fuzzy logic (FL) is the most successful controller used for this system. The mean values of 2-DOF PI and fractional PID controllers were very close to each other and yielded an average result. When the largest fluctuations in the selected regions are averaged, the PI controller gave the worst response.

This is because there are three unknown and constantly changing situations in the system. The success of conventional controllers in systems above the second order is decreasing. Well-designed fuzzy logic-based control systems have proven to react more quickly to sudden changes in error.

The most important contribution of this study is that a designed photovoltaic power generation and motor load-dependent system has shown the best push-pull converter and controller pair that will provide reference voltage under two different influences. These adverse effects are variable sunlight radiation and variable motor load. Controllers are based on PI, Fuzzy, fuzzy-tuned PI, 2-DOF PI, and fractional PID.

Data Availability

The MATLAB/SIMULINK data used to support the findings of this study are included within the supplementary information file. The MATLAB/SIMULINK file, which contains the simulation of the proposed system, was sent to International Journal of Photoenergy as a supplementary material.

Conflicts of Interest

The author declares that he has no conflicts of interest.

Acknowledgments

This study was supported by Giresun University Scientific Research Projects Unit (BAP) under grant no FEN-BAP-A-101016-140. The authors would like to thank their contribution.

Supplementary Materials

A general connection diagram of the designed system in MATLAB/Simulink environment is given with supplementary file. In this diagram, solar panels, five different controllers, push-pull converter, DC motor, and reference manufacturer signals are given. Especially, the design of the controller parts is very successful. *(Supplementary Materials)*

References

[1] I. H. Altas and A. M. Sharaf, "A novel on-line MPP search algorithm for PV arrays," *IEEE Transactions on Energy Conversion*, vol. 11, no. 4, pp. 748–754, 1996.

[2] T. D. Lee and A. U. Ebong, "A review of thin film solar cell technologies and challenges," *Renewable and Sustainable Energy Reviews*, vol. 70, pp. 1286–1297, 2017.

[3] J. Prayeen and V. VijayaRamaraju, "Materials for Optimizing Efficiencies of Solar Photovoltaic Panels," *Materials Today: Proceedings*, vol. 4, no. 4, Part D, pp. 5233–5238, 2017.

[4] K. Yanmaz, I. H. Altas, and O. O. Mengi, "Five level cascaded H-bridge D-STATCOM using a new fuzzy and PI controllers model for wind energy systems," *Advances in Electrical and Computer Engineering*, vol. 17, no. 4, pp. 49–58, 2017.

[5] Z. Wu, C. Xu, and Y. Yang, "Adjustable PID control based on adaptive internal model and application in current shared control of multi inverters," *Journal of the Franklin Institute*, vol. 354, no. 7, pp. 2699–2711, 2017.

[6] A. Saygın and A. Kerem, "Fuzzy logic based control of a loaded asynchronous motor using a 6-switched 3-level inverter," in *2017 18th International Conference Computational Problems of Electrical Engineering (CPEE)*, pp. 1–4, Kutna Hora, Czech Republic, September 2017.

[7] I. Rasoanarivo, K. Arab-Tehrani, and F. M. Sargos, "Fractional order PID and modulated hysteresis for high performance current control in multilevel inverters," *IEEE industry applications society annual meeting (IAS)*, 2011, pp. 1–7, Orlando, FL, USA, October 2011.

[8] H. Soliman, I. Abdelsalam, H. Wang, and F. Blaabjerg, "Artificial neural network based DC-link capacitance estimation in a diode-bridge front-end inverter system," in *2017 IEEE 3rd International Future Energy Electronics Conference and ECCE Asia (IFEEC 2017 - ECCE Asia)*, pp. 196–201, Kaohsiung, Taiwan, June 2017.

[9] M. R. B. Fathima, P. M. J. Princy, and S. R. Prasath, "Mathematical modeling of SVPWM ınverter fed 3 phase induction motor vector control in MATLAB/Simulink environment," in *2017 International Conference on Circuit, Power and Computing Technologies (ICCPCT)*, pp. 1–8, Kollam, India, April 2017.

[10] J. Su and D. Sun, "Model predictive torque-vector control for four-switch three-phase inverter-fed PMSM with capacitor voltage offset suppression," in *Electrical Machines and Systems (ICEMS)*, pp. 1–5, Sydney, New South Wales, Australia, August 2017.

[11] S. Qian, Y. Ye, H. Wu, and Z. Zhuang, "Optimizing PWM switching sequence of inverters using an immune genetic algorithm," in *2016 8th International Conference on Intelligent Human-Machine Systems and Cybernetics (IHMSC)*, pp. 7–10, Hangzhou, China, August 2016.

[12] I. H. Altas and A. M. Sharaf, "A photovoltaic array simulation model for Matlab-Simulink GUI environment," in *2007 International Conference on Clean Electrical Power (ICCEP'07)*, pp. 341–345, Capri, Italy, May 2007.

[13] I. H. Altas and A. M. Sharaf, "A novel maximum power fuzzy logic controller for photovoltaic solar energy systems," *Renewable Energy*, vol. 33, no. 3, pp. 388–399, 2008.

[14] G. Bayrak and M. Cebeci, "3.6 kW gücündeki fotovoltaik generatörün matlab simulink ile modellenmesi," *Erciyes Üniversitesi Fen Bilimleri Enstitüsü Fen Bilimleri Dergisi*, vol. 28, no. 3, pp. 198–204, 2012.

[15] H. Felten, A. Kreutzmann, and P. Welter, "Increase in grid-connected pv system power in germany," in *2006 IEEE 4th World Conference on Photovoltaic Energy Conference*, vol. 2, pp. 2494–2496, Waikoloa, HI, USA, May 2006.

[16] M. A. S. Masoum, H. Dehbonei, and E. F. Fuchs, "Theoretical and experimental analyses of photovoltaic systems with voltageand current-based maximum power-point tracking," *IEEE Transactions on Energy Conversion*, vol. 17, no. 4, pp. 514–522, 2002.

[17] H. Zenk, "In push-pull converter output voltage stability comparison with using fuzzy logic, PI and PID controllers," *International Journal of Engineering Research and Management (IJERM)*, vol. 3, no. 12, pp. 1–6, 2016.

[18] P. Petit, M. Aillerie, J. P. Sawicki, and J. P. Charles, "Push-pull converter for high efficiency photovoltaic conversion," *Energy Procedia*, vol. 18, pp. 1583–1592, 2012.

[19] L. A. Zadeh, "Outline of a new approach to the analysis of complex systems and decision processes," *IEEE Transactions on Systems, Man, and Cybernetics*, vol. SMC-3, no. 1, pp. 28–44, 1973.

[20] L. X. Wang, "Stable adaptive fuzzy control of nonlinear systems," *IEEE Transactions on Fuzzy Systems*, vol. 1, no. 2, pp. 146–155, 1993.

[21] A. K. Pal and I. Naskar, "Design of self-tuning fuzzy PI controller in LabVIEW for control of a real time process," *International Journal of Electronics and Computer Science Engineering*, vol. 2, no. 2, pp. 538–545, 2013.

[22] V. M. Alfaro and V. Ramon, *Model-Reference Robust Tuning of PID Controllers*, Springer, Berlin, Germany, 2016.

[23] R. Gorez, "New design relations for 2-DOF PID-like control systems," *Automatica*, vol. 39, no. 5, pp. 901–908, 2003.

[24] N. Bianchi, S. Bolognani, and F. Luise, "High speed drive using a slotless PM motor," *IEEE Transactions on Power Electronics*, vol. 21, no. 4, pp. 1083–1090, 2006.

[25] A. Damiano, G. Gatto, A. Pisano, and E. Usai, "Digital second order sliding mode control of PM DC motor," , 1999*ISIE '99. Proceedings of the IEEE International Symposium on Industrial Electronics (Cat. No.99TH8465)*, vol. 1, 1999, Bled, Slovenia, Slovenia, July 1999, 1999.

[26] İ. Eminoğlu and İ. H. Altaş, "The effects of the number of rules on the output of a fuzzy logic controller employed to a PM d.c. motor," *Computers & Electrical Engineering*, vol. 24, no. 3-4, pp. 245–261, 1998.

[27] V. M. Alfaro, R. Vilanova, and O. Arrieta, "Robust tuning of two-degree-of-freedom (2-DoF) PI/PID based cascade control systems," *Journal of Process Control*, vol. 19, no. 10, pp. 1658–1670, 2009.

[28] I. Podlubny, *Fractional differential equations: an introduction to fractional derivatives, fractional differential equations, to methods of their solution and some of their applications*, vol. 198, Elsevier, 1998.

[29] P. Shah and S. Agashe, "Review of fractional PID controller," *Mechatronics*, vol. 38, pp. 29–41, 2016.

[30] I. Rasoanarivo and F. M. Sargos, "Multi-objective analysis for designing and controlling micro-grids under multi-control with PID, MHCC and FOPID controllers," in *2013 IEEE Industry Applications Society Annual Meeting*, pp. 1–8, Lake Buena Vista, FL, USA, October 2013.

[31] A. Tepljakov, E. Petlenkov, and J. Belikov, "FOMCON: fractional-order modeling and control toolbox for MATLAB," in *2011 Proceedings of the 18th International Conference Mixed Design of Integrated Circuits and Systems-MIXDES 2011*, pp. 684–689, Gliwice, Poland, June 2011.

[32] N. Rajarajeswari and K. Thanushkodi, "Bi-directional DC–DC converter with adaptive fuzzy logic controller," *Elektronika ir Elektrotechnika*, vol. 89, no. 1, pp. 65–68, 2009.

[33] C. L. Trujillo, D. Velasco, E. Figueres, G. Garcerá, and R. Ortega, "Modeling and control of a push-pull converter for photovoltaic microinverters operating in island mode," *Applied Energy*, vol. 88, no. 8, pp. 2824–2834, 2011.

[34] O. O. Mengi, "A Five-Level H-Bridge STATCOM for an Off-Grid PV Solar Farm under Two Controllers PI and PIλ-MPC Hybrid," *International Journal of Photoenergy*, vol. 2018, Article ID 4030214, 14 pages, 2018.